One-pot synthesis of ZnO nanoparticles supported on halloysite nanotubes for catalytic applications

Marina Massaro,[a,*] Michele Casiello,[b] Lucia D'Accolti,[b] Giuseppe Lazzara,[c] Angelo Nacci,[b] Giuseppe Nicotra,[d] Renato Noto,[a] Alberto Pettignano,[c] Corrado Spinella[d] and Serena Riela[a,*]

[a] Dipartimento STEBICEF, Sez. Chimica, Università degli Studi di Palermo, Viale delle Scienze, Ed. 17, 90128 Palermo, Italy. E-mail: marina.massaro@unipa.it; serena.riela@unipa.it

[b] Chemistry Department, University of Bari "Aldo Moro" via Orabona 4, 70126 Bari, Italy.

[c] Dipartimento di Fisica e Chimica, Università degli Studi di Palermo, Viale delle Scienze, Ed. 17, 90128 Palermo, Italy.

[d] CNR-IMM, Zona Industriale Strada VIII, 5, 95121 Catania, Italy.

KEYWORDS. halloysite nanotubes, zinc oxide, heterogeneous catalyst, photodegradation reaction, biodiesel production.

ABSTRACT. A novel versatile catalyst based on halloysite and zinc oxide (HNT@ZnO) was prepared and characterized. It was found that the presence of halloysite improved the UV-*vis* spectral absorption ability of ZnO. The hybrid was successful used as photocatalyst for the methylorange and rhodamine B degradation. In addition, after eight consecutive cycles for the methylorange photodegradation, the hybrid did not exhibit significant reduction in its photocatalytic performances confirming its stability. Based on trapping experiments and calculated energy bands we also proposed a photocatalytic mechanism.

Furthermore, to evaluate the versatility of the synthetized HNT@ZnO hybrid, we used it as catalyst for biodiesel production from soybean oil, too. Also, in this case, the hybrid showed good catalytic performance and recyclability.

1. Introduction

Nanomaterials in the form of solid support have been widely deployed as sustainable nanocatalysts to confront various sustainable issues in catalysis. Heterogeneous catalysts, indeed, have been widely used in chemical and petrochemical processes due to their versatility, easiness of recovery and recyclability. Among the different nanomaterials that are currently employed to this purpose, halloysite nanotubes (HNTs) possess several advantages, including high stability, resistance against organic solvents, ease of disposal or reusability and they are available in tons at low cost.

Generally, HNTs consist of an inner lumen composed of aluminol groups and an external surface constituted by siloxane groups. Due to this peculiar chemical composition, halloysite possesses different charged surfaces: positive on the internal surface and negative in the external one in a wide pH range (Bretti et al., 2016). Halloysite has found application as nanocontainers for biologically active molecules (Massaro et al., 2018a; Massaro et al., 2018c; Massaro and Riela, 2018; Massaro et al., 2019a; Tarasova et al., 2019), adsorbent nanomaterials for wastewater decontamination (Massaro et al., 2016; Cataldo et al., 2018; Gładysz-Płaska et al., 2018), nanofiller to improve polymer performances (De Silva et al., 2018; Kumar et al., 2019; Sharma et al., 2019) and supports for catalytic species (Li et al., 2015b; Sidorenko et al., 2018; Massaro et al., 2019b; Mishra and Mukhopadhyay, 2019). In this context several metal nanoparticles have been successfully immobilized on halloysite surfaces, obtaining extremely active nanocatalysts for several organic reactions (Massaro et al., 2017; Massaro et al., 2018b).

ZnO nanomaterials have gained considerable attention due to their physical and chemical properties such as low cost, no toxicity and chemical stability. In addition, due to their amphoteric nature, ZnO has been widely utilized for different catalytic purposes including wastewater treatments (Cantarella et al., 2018; Ta et al., 2019) and some organic reactions (Gade et al., 2017; Kong et al., 2017).

Although several studies report the immobilization of metal nanoparticles on HNTs, only a limited number of reports are available in the literature on the deposition of ZnO on halloysite and most of them envisage the in situ formation of nanostructured forms of ZnO by calcination of suitable zinc salts which could result time-consuming (De Silva et al., 2015; Li et al., 2015a; Shankar et al., 2018). To date, no studies have been reported on the deposition of ZnO on HNT external surface of its commercial bulk form, and very few reports study the catalytic

performances of the ZnO based catalyst both in the photodegradation of organic pollutants and in organic reactions.

Herein we report the synthesis and characterization of a nanocatalyst based on HNTs and ZnO (HNT@ZnO). To evaluate the feasibility of the hybrid as a catalyst, we studied the photodegradation of organic dyes, using rhodamine B and methyl orange as models. We also investigated the recyclability of the system and proposed a photodegradation mechanism.

Finally, to estimate the versatility of the novel HNT@ZnO catalyst, we have also performed preliminary investigations for biodiesel production from soybean oil.

2. **Materials and Methods**

All reagents needed for the synthesis of the HNT@ZnO nanocatalyst were purchased from Sigma-Aldrich and used without further purification.

Standard solutions of Zn^{2+} ion used for calibration curve (concentration range 0.2 – 20 mg L^{-1}) were prepared by diluting a Carlo Erba 1 g L^{-1} standard solution in 2% HCl (purity 99.99 %). All the solutions were prepared using freshly CO_2-free ultra-pure water ($\rho \geq 18$ MΩ cm).

UV–visible measurements were performed using a Beckmann DU 650 spectrometer.

GC/MS experiments were run on a Shimadzu GLC 17-A instrument connected with a Shimadzu QP5050A selective mass detector using an SLB-5MS column (30 m × 0.25 mm id, film thickness 0.25 μm).

FT-IR spectra (KBr) were recorded with an Agilent Technologies Cary 630 FT-IR spectrometer. Specimens for these measurements were prepared by mixing 5 mg of the sample powder with 100 mg of KBr.

An AESEM FEI QUANTA 200F microscope apparatus, with an EDS probe, was used to study the morphology of the functionalized HNTs. Before each experiment, the sample was coated with gold under argon by means of an Edwards Sputter Coater S150A in order to avoid charging under the electron beam.

The Zn^{2+} concentration in the samples was measured by Inductively Coupled Plasma Optical Emission Spectroscopy (ICP-OES) technique. An ICP-OES Perkin Elmer, Model Optima 2100, equipped with an auto sampler model AS-90 was used. The zinc emission intensity was measured at two wavelengths (213.857 and 202.548 nm) and each measurement was repeated three times.

Photochemical reactions were performed in aqueous solution by using a Rayonet photoreactor fitted with 8 W Hg lamp irradiating at 365 nm (in 15 mL Pyrex vessels) and a merry-go-round apparatus.

TEM analyses were performed with a JEOL ARM200F Cs-corrected, operated at 200 keV; the images were acquired in scanning mode (S/TEM) and with an High Angle Annular Dark Field detectors (HAADF).

2.1. Synthesis of HNT@ZnO

HNT@ZnO hybrid was prepared by mixing 1 g of ZnO nanoparticles and 1 g of HNTs in 30 mL of phosphate buffer solution (0.01 M) at pH 8.0. The mixture was stirred for 24 h at room temperature. Afterwards, the dispersion was centrifuged and the solid precipitate was washed several times with deionized water (ca. 200 mL). The white powder obtained was dried at 60 °C overnight.

2.2. Photocatalytic measurements

The photocatalytic activity of HNT@ZnO hybrid was evaluated by monitoring the photocatalytic degradation of organic dye molecules (MO and RhB) in aqueous solutions under UV/Vis-light irradiation under a neutral pH condition. For each photocatalytic experiment, different amounts of the HNT@ZnO hybrid (ranging from 5 to 25 mg mL^{-1}) were added into 1×10^{-2} M organic dye aqueous solution (2 mL) in a quartz glass reactor. Prior to irradiation, the suspension was magnetically stirred in the dark for 20 min to achieve the adsorption–desorption equilibrium. After the appropriate time, the dispersion was centrifuged and the aqueous supernatant was collected. To estimate the degree of degradation, the supernatant was detected by measuring the maximum absorbance at 460 and 550 nm for MO and RhB, respectively to evaluate the concentration of the dyes.

To test the stability of the HNT@ZnO hybrid, the collected powder was washed three times with water, dried and used for another catalytic reaction. This process was repeated at least for eight times.

2.3. Transesterification Experiments

Procedure adapted from the Lit.(Casiello et al., 2019) In a typical experiment, a 10 mL glass vial equipped with a magnetic bar was charged with Methanol (4 mL), 0.5 mL of commercial soybean oil (415 mg at 25 °C), TBAI (123 mg, 30% w/w) and HNT@ZnO (9 mg, 2% w/w). Then, the vial was sealed, heated at 70 °C under stirring and left to react for the proper time (7 hours). Next, reaction mixture was cooled to room temperature, transferred into a centrifuge tube and subjected to 3500 rpm for 15 min. A pale brown solid HNT@ZnO layered to the bottom, a residual oily phase above (which was absent in the case of complete conversion), and an upper methanolic phase were commonly visible after centrifugation.

The supernatant methanolic solution (containing FAMEs, glycerol and TBAI co-catalyst) was roughly separated by means of a Pasteur pipette. The lower biphasic residue (HNT@ZnO + unreacted oil) was washed twice with 2 mL of fresh methanol to remove traces of biodiesel and TBAI (by stirring and centrifuging the mixture after each addition of MeOH). The combined methanolic phases (washing fractions and post-reaction solution) were subjected to the separation step of TBAI and glycerol, followed by FAMEs qualitative and quantitative analyses.

Biphasic residue (HNT@ZnO + unreacted oil), after washing with MeOH, was treated twice with ethyl acetate (2 mL) and centrifugated. The combined supernatants were evaporated, and the oil residue weighed for determining the conversion (alternatively, conversion was evaluated by ^{1}HNMR). The remaining solid HNT@ZnO was washed with acetone, filtered and dried in an oven at 80 ° C for 4 hours, prompt to be reused in a further run (for recycling experiments).

For FAMEs analyses, the methanolic phase (FAMEs + glycerol + TBAI) was added with 50 mg of methyl heptadecanoate as an internal standard, evaporated to small volume and suspended into 10 mL of ethyl acetate. This caused the precipitation of TBAI that was filtered off and totally recovered in high purity (ascertained by ^{1}HNMR). The ethyl acetate solution was evaporated to small volume with separation of small drops of a viscous phase due to glycerol, that was removed by washing with water. After drying, ethyl acetate solution was subjected to qualitative and quantitative analyses (by GC-MS) to identify FAMEs and determine composition of the biodiesel product according to the previously reported procedures.(Casiello et al., 2019)

3. Results and Discussion

The HNT@ZnO catalyst was obtained by immobilization of ZnO nanoparticles on halloysite nanotubes. In particular, to an aqueous suspension of ZnO nanoparticles (phosphate buffer solution pH = 8.0) was added pristine HNTs powder. The obtained dispersion was stirred for 24

h, at room temperature and then the solid powder was filtered off and washed several times to remove the unreacted ZnO nanoparticles.

The content of ZnO on the solid halloysite support was determined using ICP-OES and the total zinc oxide amount was estimated as 7.5 wt%. As shown in the EDS pattern, beside the silicon and aluminum elements existing in halloysite, the presence of evenly distributed signals from Zn further confirmed the presence of ZnO in the sample. The SEM micrograph (see SI) showed that the characteristic lengths and the tubular shape of HNTs were preserved in the HNT@ZnO catalyst and the tubes surface appears smoothed as a consequence of the ZnO nanoparticles deposition.

Further confirmation of the presence of ZnO nanoparticles onto the solid support was provided by FT-IR spectroscopy. In Figure 1b is reported the FT-IR spectrum of the HNT@ZnO nanomaterial and for comparison that of pristine halloysite. As it is possible to observe all characteristic vibration bands of HNTs are present (Massaro et al., 2018c) and no shift in their position was observed, indicating that the nanoparticles were deposited onto the external HNT surface. In addition, it is possible to observe in the HNT@ZnO spectrum the presence of a signal at ca. 470 nm, due to the stretching vibration of the Zn-O group (Li et al., 2015a).

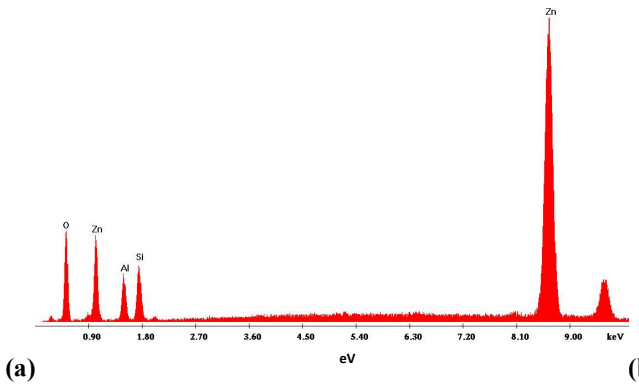

(a)

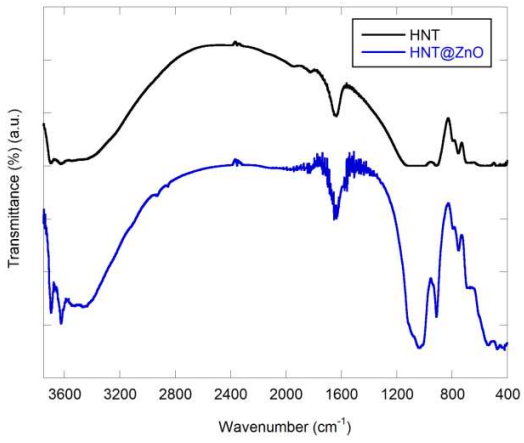

(b)

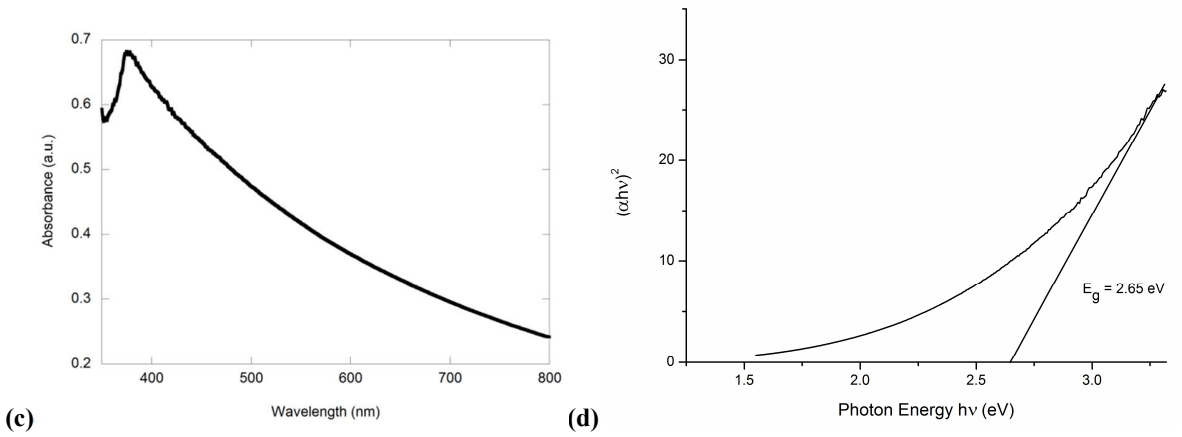

Figure 1. (a) EDS pattern; (b) FT-IR spectra; (c) UV-*vis* spectrum and (d) Tauc plot for HNT@ZnO hybrid.

In Figure 1c is reported the UV-*vis* spectrum of the HNT@ZnO nanomaterial. The study of the optical absorption of a semiconductor material is, indeed, important as far as is concerned its application as photocatalyst.

It is known that pure ZnO shows an optical absorbance in the UV region exhibiting an abrupt onset of absorption at about 387 nm, which corresponds to a band gap of about 3.2 eV, which is in a good agreement with literature reports (Ma et al., 2018). By supporting the ZnO nanoparticles on HNTs, it was observed a main absorption maximum at ca. 370 nm, which corresponds to the main electronic transition from valence band to conduction band(Iqbal et al., 2018) and an absorption offset at ca. 420 nm. The band gap energy of the HNT@ZnO nanomaterial can be calculated by the Tauc plot (Figure 1d), from the x-axis intercepts of the tangent lines of the curve obtained by plotting the $(\alpha h\nu)^2$ as a function of the photo energy ($h\nu$) (Anandan et al., 2010). The E_g value was found to be 2.65 eV. This difference in the E_g values is probably due to the HNT presence. In particular, we hypothesize a synergistic effect between ZnO nanoparticles and HNTs which could produce an overlapping of energy levels, thus a decreasing of the conduction band minimum and an increasing of the valence band maximum. valence band maximum. On the other hand, this variation may reflect the sintering of nanoparticles onto the HNTs surface. Nevertheless, regardless on the actual mechanism of band gap shift, the nanomaterial obtained in the present study could show enhanced photocatalytic activity.

Z-contrast Scanning Transmission Electron Microscopy (S/TEM) images showed that the morphology of the HNT@ZnO hybrid did not present any significant change after the immobilization of the ZnO nanoparticles. As it is possible to observe from Figure 2a-b the hybrid possesses a tubular hollow structure with an empty lumen. However, the external HNT surfaces are rougher and less defined with respect to those of pristine nanotubes, indicative of a partial coating with the nanoparticles. The ZnO nanoparticles, clearly visible since their brighter intensity due their higher atomic number Z, were uniformly distributed and well dispersed on the support. From statistical analysis, the HNT@ZnO material showed the presence of small ZnO nanoparticles with an average diameter of 2.4 ± 0.5 nm and narrow size distribution (Figure 2c). Zn atoms, in ZnO nanoparticles, have been clearly reveled by punctual X-ray chemical analysis. Here the characteristic emitted by the specimen after the interaction with the scanning electron beam, are collected in a region containing the nanoparticles, such as the one within the red square (see figure 2d), and a 2D chemical map (image in red colour) is then obtained by extracting pixel by pixel the corresponding Zn K_{α},K_{β} X-rays in the same area.

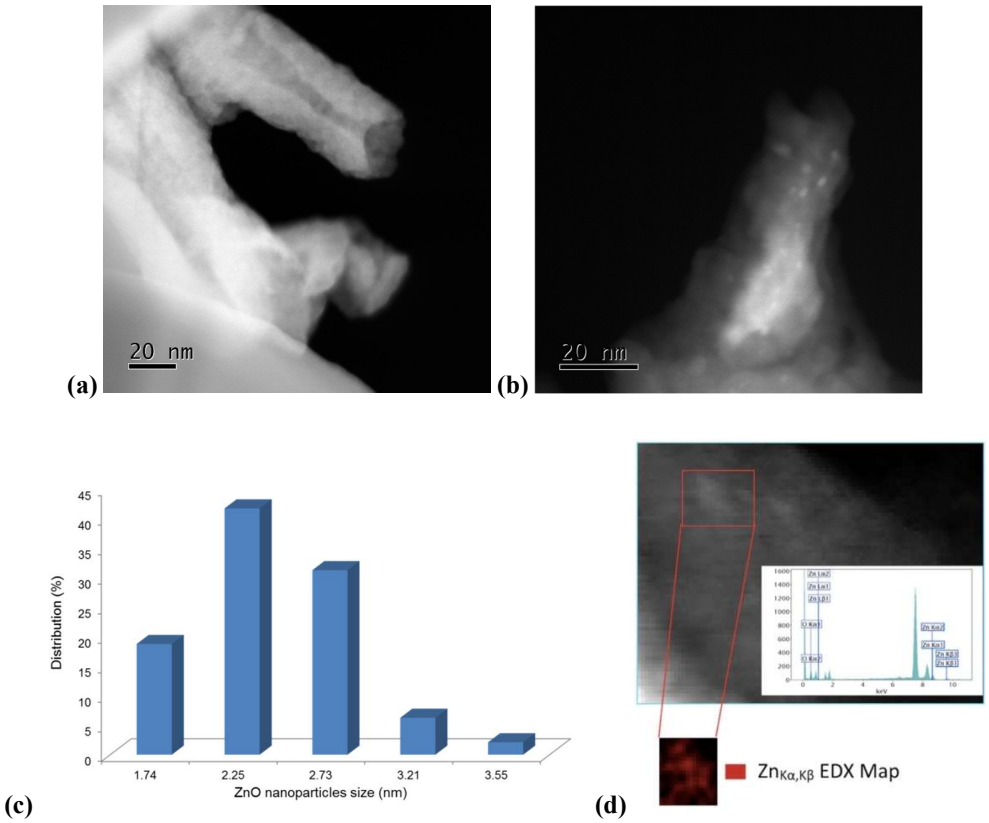

Figure 2. (a-b) Z-Contrast S/TEM images showing a HNT@ZnO; (c) ZnO nanoparticles size distribution (n = 50); (d) Z-Contrast S/TEM image and chemical map of Zn (image in red) obtained by collecting the characteristic X-ray

Zn K_{α},K_{β} coming up from the region inside the red square. The integrated EDX spectrum within the same area is even reported in the inset of the figure.

3.1. Photocatalytic performances of the HNT@ZnO nanomaterial

The photocatalytic activity of as-obtained HNT@ZnO nanohybrid was evaluated by photodegradation of 5 ppm of rhodamine B (RhB) and methyl orange (MO), chosen as models, under visible light irradiation. The two dyes were chosen since they possess different charge in the experimental conditions adopted in the photocatalytic tests. This aspect should highlight some selectivity of the HNT@ZnO based on electrostatic interactions which could arise between the dyes and the HNT surfaces.

The aqueous dispersions of HNT@ZnO hybrid and the dye were stirred in the dark for ca. 20 min, to reach adsorption/desorption equilibrium before starting the photocatalytic tests. In these conditions, the hybrid did not show any dye adsorption (<5%), and the direct photolysis of the two dyes was also insignificant.

Photocatalytic tests were performed taking into account the effects of both pristine HNTs and HNT@ZnO catalyst.

First of all, the photodegradation reaction was followed in absence of ZnO nanoparticles. By adding different amounts of pristine HNT to the dye solution, no reduction of both dyes occurred over the time. On the contrary, with the addition of the HNT@ZnO hybrid, the photodegradation occured in few minutes. The photocatalytic efficiency was expressed as the C_t/C_0 ratio over the time (Figure 3), where C_0 and C_t are the concentration of the dye (M) at different irradiation time of t_0 and t.

In Figure 3a is reported the time-dependent photocatalytic degradation of RhB in the presence of different amount of HNT@ZnO (ranging from 5 to 25 mg mL^{-1}). As it is possible to observe, no significant differences in the photocatalytic activity were observed in all cases investigated and the dye was quantitatively degraded after 30 min of irradiation, indicating the efficiency of the catalyst in the degradation of organic pollutant.

On the other hand, as it is possible to observe from Figure 3b, the introduction of the HNT@ZnO nanomaterial to a MO solution, led to an increase in the reaction rate and the dye was completely degraded after only 3 min in all range of concentration of catalyst investigated.

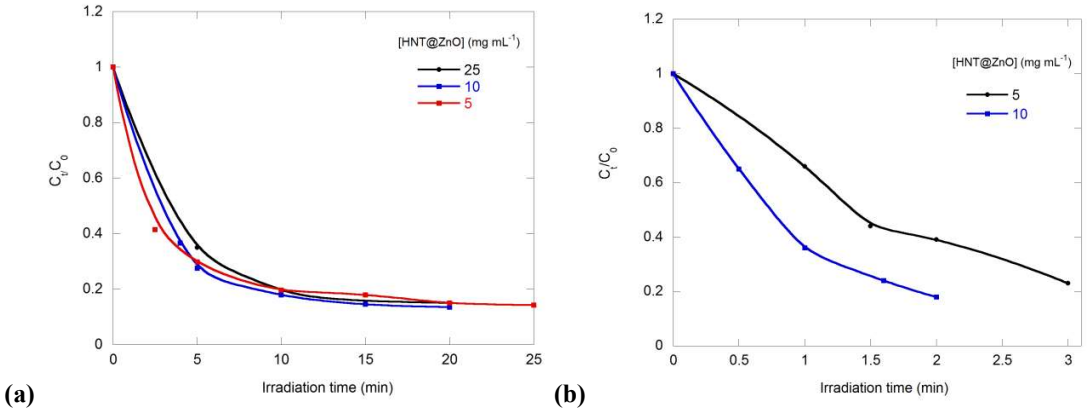

Figure 3. Rhodamine B (a), and MO (b) photodegradation under UV light irradiation for HNT@ZnO.

In order to compare the photocatalytic activity of the obtained material towards the two dyes, the kinetic constants were calculated by applying the Langmuir–Hinshelwood model,(Niu et al., 2015) as expressed by the following equation:

$$\ln\left(\frac{C_t}{C_0}\right) = -kt \qquad \text{(Eq. 1)}$$

where k is the pseudo-first-order rate constant of photodegradation (min^{-1}).

The kinetic constants obtained are reported in Table 1.

Table 1. Rate parameters of photo-catalytic activity of HNT@ZnO towards MO and RhB dye.[a]

Entry	[HNT@ZnO] (mg mL^{-1})	k (min^{-1})
RhB		
1	5	$(3.0 \pm 0.5) \times 10^{-2}$
2	10	$(5.0 \pm 1) \times 10^{-2}$
3	25	$(1.54 \pm 0.02) \times 10^{-1}$
MO		
4	5	0.49 ± 0.06
5	10	1.3 ± 0.3
6[b]	10	$(1.09 \pm 0.09) \times 10^{-2}$

[a] [dye] = 1×10^{-5} M; V_f = 2 mL. [b] [dye] = 1×10^{-3} M.

As expected, an increase in the HNT@ZnO concentration resulted in a substantial improvement in photocatalytic performances for both dyes. Furthermore, in all cases investigated the kinetic of degradation of MO is faster than that of RhB. Indeed, we found a kinetic constant ca. 16 times

higher for the MO photodegradation with respect to that of the RhB by keeping the catalyst concentration constant (entries 1 and 4). By increasing the dye concentration (from 5 to 500 ppm), we observe a decrease in the kinetic constant value as a consequence of the saturation of the reactive sites on the catalyst surface (entry 6). The different behavior of the two dyes could be explained considering the chemical features of HNT. Halloysite could significantly attract the negatively charged methyl orange into the positively charged lumen through both electrostatic and hydrophobic interactions, resulting in its enrichment on the HNT@ZnO surface. At pH values up to 7.4, RhB mainly exists in zwitterion forms forming dimers which can partially be absorbed on the catalyst surfaces, resulting in a slower photodegradation process.

The obtained results show that HNT@ZnO hybrid could be used as a good photocatalyst for the degradation of anionic dyes with respect to the neutral ones in a pH 7.0 solution.

3.1.2. Recyclability

Figure 4a displays the recyclability of HNT@ZnO nanomaterial (180 mg) for the degradation of MO (1×10^{-4} M). After each cyclic run under light illumination, the catalyst was separated from the dispersion by centrifugation and washed several times with water. The recovered HNT@ZnO nanomaterial was again added to a fresh MO solution and its photocatalytic efficiency was evaluated. It is found that the photocatalytic performance of the HNT@ZnO remains almost unchanged even after eight cycles of runs, demonstrating that the nanomaterial exhibited high recyclability.

TEM analyses were performed on the reused catalyst to verify its stability. Figure 4b shows S/TEM image of the catalyst recorded after eight consecutive cycles showing a ZnO nanoparticles slightly bigger in size with respect to those of fresh catalyst. By statistical analysis, it was found that the mean ZnO diameter was ca. 3.9 ± 0.8 nm. To the light of these results it is plausible to hypothesize a “release and catch” mechanism, where the ZnO nanoparticles are released in solution during the photocatalytic process and, after the reaction, they are redeposited on the solid support.

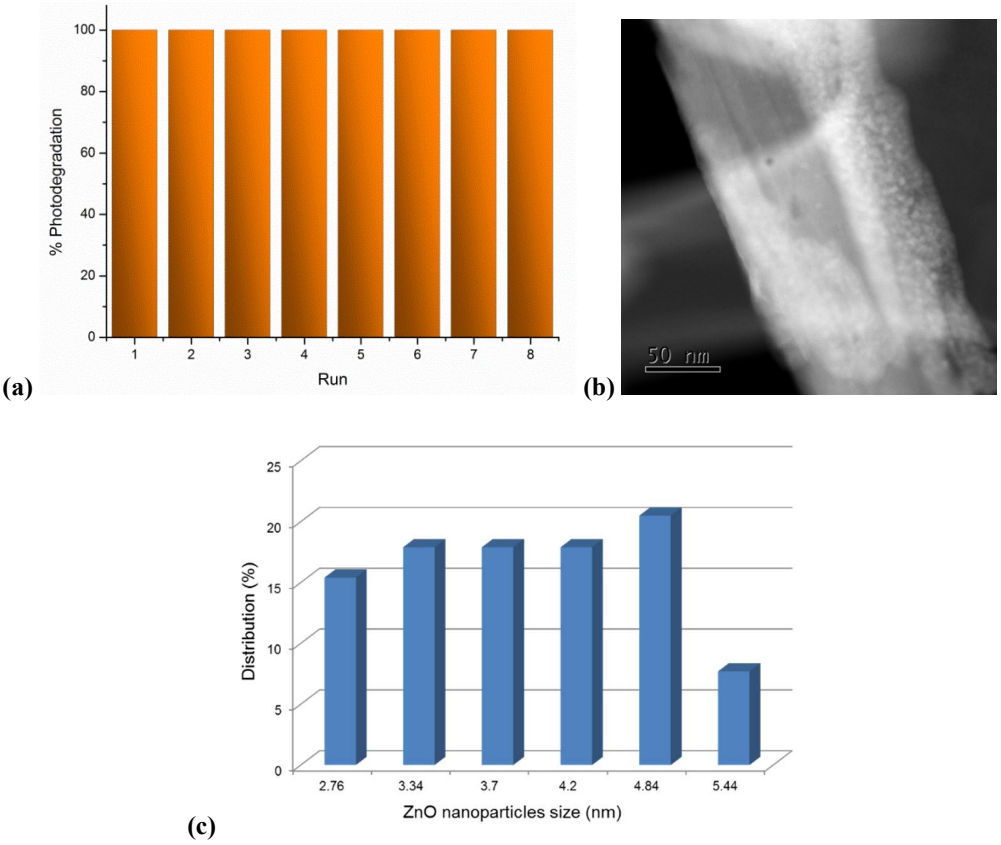

Figure 4. (a) Recycling tests of HNT@ZnO hybrid; (b) S/TEM images of the catalyst after eight consecutive runs; (c) ZnO nanoparticles size distribution (n = 50).

3.1.3. Trapping experiments and proposed photodegradation mechanism

To shed some light on the probable mechanisms involved in the dye's degradation, some active species trapping experiments were performed by adding to a RhB/HNT@ZnO dispersion trapping scavengers. In particular, among the different kinds of scavengers the isopropyl alcohol (IPA), triethanolamine (TEOA) and p-benzoquinone (BQ) were chosen as model for the detection of hydroxyl radical (·OH), holes (h^+) and superoxide radical ($O_2^{-\cdot}$), respectively. The obtained results are showed in Figure 5.

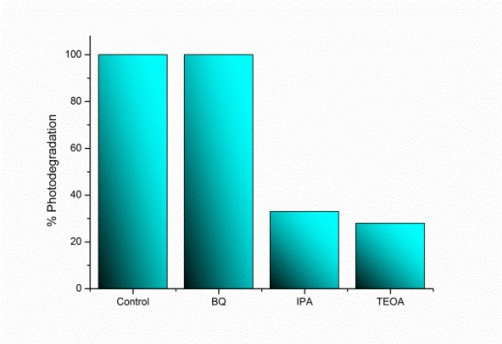

Figure 5. Effects of scavengers on the photocatalytic efficiency of HNT@ZnO hybrid.

The results showed that after the addition of 1 mmol of BQ, no inhibition of the RhB photodegradation rate occurred, indicating that superoxide radical ($O_2^{-\cdot}$) did not dominate the photodegradation process of the HNT@ZnO catalyst. On the contrary, the photodegradation rate decreases by adding both IPA and TEOA (33% and 28%, respectively). Therefore, it is plausible to conclude that holes and hydroxyl radicals play an active role in the degradation process.

To confirm the experimental findings and to propose a plausible mechanism for the photocatalytic degradation of dyes in the presence of the HNT@ZnO nanomaterial, the relative energy levels of valence band maximum (VB) and conduction band minimum (CB) should be calculated since they would be significant for the redox capacity of photoinduced carriers in the photocatalytic system. Generally, the CB and VB of a semiconductor can be calculated via the empirical equation:

$$E_{VB} = \chi - E_e + 0.5E_g$$

$$E_{CB} = E_{VB} - E_g$$

where E_{VB} is the valence band (VB) potential, E_{CB} is the conduction band (CB) potential, χ is the absolute electronegativity of a semiconductor, which is the geometric mean of the absolute electronegativity of the constituent atoms (defined as the arithmetic mean of the atomic electron affinity and the first ionization energy), and for ZnO, is 5.79 eV, E_E is the energy of free electrons on the hydrogen scale (ca. 4.5 eV) and E_g is the band gap of the semiconductor.

The VB potential of the HNT@ZnO was found to be 2.61 eV, which resulted more positive than the standard reaction potential of the ·OH/H_2O (2.27 vs. NHE), therefore it is plausible that the separated photogenerated holes (h_{VB}^+) can react with H_2O to form the hydroxyl radical ·OH. The

CB potential, instead, was -0.035 eV, less negative than the $E^0_{O_2/O_2^{-\cdot}}$ (-0.33 eV vs. NHE) and thus, the e^-_{CB} on the surface of the hybrid are not able to reduce O_2 to $O_2^{-\cdot}$.

In summary, the light irradiation activates ZnO to generate strongly oxidative holes (h^+_{VB}) in valence band and reductive electrons (e^-_{CB}) in conduction band. The h^+_{VB} can react with H_2O forming a free radical ·OH and H^+, and H^+ subsequently react with the absorbed O_2 to yield ·OH, which are responsible of the dye degradation according to the trapping experiment. Similar results were obtained from TiO_2 nanoparticles supported on HNT (Wang et al., 2011).

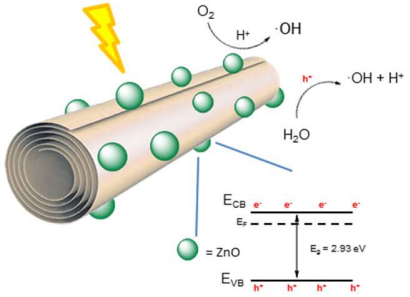

Figure 6. Illustration of the photocatalytic degradation mechanism of HNT@ZnO hybrid.

3.2. Transesterification reaction: preliminary investigation for biodiesel production

Fatty acid methyl esters (FAMEs), namely biodiesel, are a well-known renewable, non-toxic, biodegradable fuel, produced by methanolysis of triglycerides (Kim et al., 2018). Among the several catalysts employed for their production, Zinc oxide has gained great attention due to the cheap, non-toxic, thermal stable, and amphoteric properties. This latter feature is particularly valuable as it enables the application to waste lipids and highly acidic unrefined feedstocks, where esterification and transesterification processes are requested to occur simultaneously (Yan et al., 2009). However, due to the low catalytic activity of ZnO_{bulk} powder, composite materials or nanostructured forms of this oxide are usually preferred, thus imposing costly, time-consuming, and tedious preparations of catalysts (e.g., calcination, microwave irradiation, etc.) (Niu et al., 2015).

In this context, the development of an efficient, recyclable and easy-to-prepare nanosized ZnO catalyst can be considered of valuable importance. Stimulated by the successful results obtained in photocatalysis, we decided to investigate the reactivity of our halloysite nanocomposite HNT@ZnO in the transesterification of triglycerides for biodiesel production.

Reaction conditions were surveyed on soybean oil as model lipid using, for comparison, the protocol adopted in our previous work based on ZnO powder catalyst and tetrabutylammonium iodide (TBAI), an additive that acted as a phase transfer agent (PTA) (Casiello et al., 2019).

As showed in Table 2, pristine halloysite support (p-HNT) displayed negligible catalytic activity, even in the presence of PTA (Table 2, entries 1-2). In contrast, HNT@ZnO nanocomposite showed an appreciable reactivity furnishing biodiesel in a 19% of yield (entry 3). This is an encouraging result if compared with the analogous based on bulk ZnO, which instead furnished a halved yield (Table 2, entry 4), especially considering that reaction conditions for HNT@ZnO catalyst in Table 2 have not been optimized.

Good performance of our nanocatalyst HNT@ZnO were further highlighted in the reaction modified with the phase transfer agent (TBAI) which afforded, similarly to the ZnO_{bulk} analogous material, the complete conversion of soybean oil into biodiesel with a 95% of yield (Table 2, entries 5-6).

Table 2. Preliminary tests in HNT@ZnO catalysed biodiesel production from soybean oil.

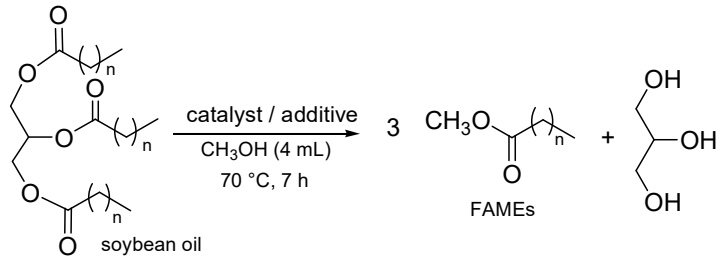

Entry	Catalyst	Additive	Conv. (%)[b]	FAMEs Yield (%)[c]
1	p-HNTs	-	5	<5
2	p-HNTs	TBAI	5	<5
3	HNT@ZnO	-	22	19
4[d]	ZnO_{bulk}	-	15	10
5	HNT@ZnO	TBAI	>99	95
6[d]	ZnO_{bulk}	TBAI	>99	96

[a] Reaction conditions: soybean oil 0.5 mL (0.415 g), methanol 4 mL, TBAI 123 mg (30% w/w), catalyst: p-HNT 100 mg, ZnO_{bulk} 9 mg (2.2% w/w), or HNT@ZnO 100 mg (loaded with 7.5 mg of ZnO, 1.8% w/w respect to soybean

oil). [b] Evaluated weighing unreacted oil; [c] Determined via GC-MS with hexadecane as an external standard. [d] Previous work results.[4]

3.2.1. Procedure for catalyst recycling

Recycling experiments were also conducted to verify the recovery of the catalyst system HNT@ZnO and assure that no residues are released into the biodiesel product during the work-up procedure.

Figure 7 shows that, after being reused 4 times, the catalyst system maintains good performance, while the slight decrease of activity is due to the loss of catalytic material during manipulations. The absence of leaching of ZnO into the biodiesel mixture was ascertained by ICP-MS.

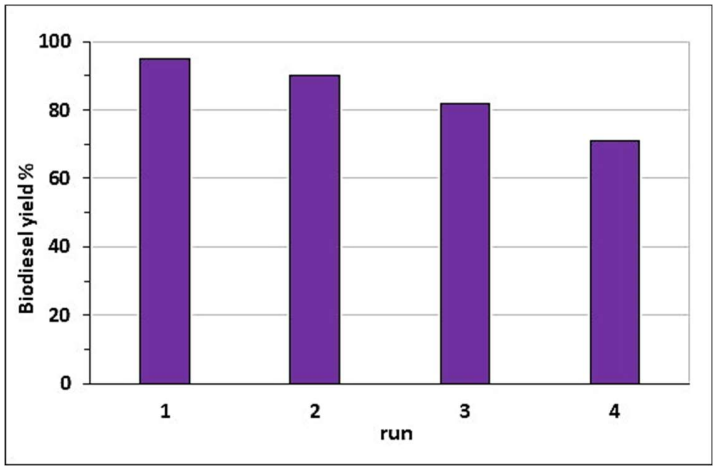

Figure 7. HNT@ZnO catalyst recycling tests in biodiesel production from soybean oil.[a]

[a] Reaction conditions: soybean oil 0.5 mL (0.415 g), methanol 4 mL, TBAI 123 mg (30% w/w), catalyst HNT@ZnO 100 mg (loaded with 7.5 mg of ZnO, 1.8% w/w respect to soybean oil). Yields determined via GC-MS with methyl heptadecanoate as an external standard (see experimental section).

In summary, from these preliminary results undoubtedly emerged the potentialities of halloysites nanocomposites HNT@ZnO as nanocatalyst in biodiesel production from soybean oil. Despite the activity seems to be similar to that of ZnO_{bulk} powder, performance of this material is susceptible of strong improvement especially considering the possibility of optimizing the reaction conditions and the opportunity of introducing on the halloysite support surface co-

catalytic functionalities (e.g. tetraalkylammonium cations). Work is in progress following this idea, in order to realize a unique, efficient, recyclable and easy-to-prepare heterogenous catalyst.

Conclusions

In summary, a heterogenous and versatile catalyst based on ZnO supported on halloysite nanotubes was synthetized and characterized. S/TEM investigations on the HNT@ZnO catalyst showed a uniformly dispersed ZnO nanoparticles on the halloysite external surface with a diameter size of ca. 2.4 nm. Furthermore, UV-*vis* studies highlighted that the presence of halloysite decreases the energy band gap of the semi-conductor if compared to the ZnO nanoparticles bulk. The catalytic performances of the hybrid were tested in the photodegradation reaction of two organic dyes, chosen as models, namely methylorange and rhodamine B under UV light and for the biodiesel production from soybean oil. In both cases we observed a very good catalytic activity of the HNT@ZnO synthetized and a good recyclability of the system without leaching of the metal. In conclusion the new catalyst, synthetized with a simple and low cost procedure, represents a versatile system which can be used for future industrial applications.

ACKNOWLEDGMENT

The authors would thank Mr. C. Caruso, Prof. A. Pace and Prof. A. Palumbo Piccionello (University of Palermo) for the photoreactor equipment. Part of this project has received funding from the European Union's Horizon 2020 research and innovation programme under grant agreement No 823717 – ESTEEM3.

REFERENCES

Anandan, S., Ohashi, N., Miyauchi, M., 2010. ZnO-based visible-light photocatalyst: Band-gap engineering and multi-electron reduction by co-catalyst. *Applied Catalysis B: Environmental*, 100, 502-509.

Bretti, C., Cataldo, S., Gianguzza, A., Lando, G., Lazzara, G., Pettignano, A., Sammartano, S., 2016. Thermodynamics of Proton Binding of Halloysite Nanotubes. *Journal of Physical Chemistry C*, 120, 7849-7859.

Cantarella, M., Di Mauro, A., Gulino, A., Spitaleri, L., Nicotra, G., Privitera, V., Impellizzeri, G., 2018. Selective photodegradation of paracetamol by molecularly imprinted ZnO nanonuts. *Applied Catalysis B: Environmental*, 238, 509-517.

Casiello, M., Catucci, L., Fracassi, F., Fusco, C., Laurenza, A.G., Di Bitonto, L., Pastore, C., D'accolti, L., Nacci, A., 2019. ZnO/ionic liquid catalyzed biodiesel production from renewable and waste lipids as feedstocks. *Catalysts*, 9.

Cataldo, S., Lazzara, G., Massaro, M., Muratore, N., Pettignano, A., Riela, S., 2018. Functionalized halloysite nanotubes for enhanced removal of lead(II) ions from aqueous solutions. *Appl. Clay Sci.*, 156, 87-95.
De Silva, R.T., Dissanayake, R.K., Mantilaka, M.M.M.G.P.G., Wijesinghe, W.P.S.L., Kaleel, S.S., Premachandra, T.N., Weerasinghe, L., Amaratunga, G.A.J., De Silva, K.M.N., 2018. Drug-Loaded Halloysite Nanotube-Reinforced Electrospun Alginate-Based Nanofibrous Scaffolds with Sustained Antimicrobial Protection. *ACS Applied Materials and Interfaces*, 10, 33913-33922.
De Silva, R.T., Pasbakhsh, P., Lee, S.M., Kit, A.Y., 2015. ZnO deposited/encapsulated halloysite-poly (lactic acid) (PLA) nanocomposites for high performance packaging films with improved mechanical and antimicrobial properties. *Appl. Clay Sci.*, 111, 10-20.
Gade, V.B., Rathi, A.K., Bhalekar, S.B., Tucek, J., Tomanec, O., Varma, R.S., Zboril, R., Shelke, S.N., Gawande, M.B., 2017. Iron-Oxide-Supported Ultrasmall ZnO Nanoparticles: Applications for Transesterification, Amidation, and O-Acylation Reactions. *ACS Sustain. Chem. Eng.*, 5, 3314-3320.
Gładysz-Płaska, A., Majdan, M., Tarasiuk, B., Sternik, D., Grabias, E., 2018. The use of halloysite functionalized with isothiouronium salts as an organic/inorganic hybrid adsorbent for uranium(VI) ions removal. *J. Hazard. Mater.*, 354, 133-144.
Iqbal, D., Sarfraz, A., Erbe, A., 2018. Gradient in defect density of ZnO nanorods grown by cathodic delamination, a corrosion process, leads to end-specific luminescence. *Nanoscale Horiz.*, 3, 58-65.
Kim, D.-S., Hanifzadeh, M., Kumar, A., 2018. Trend of biodiesel feedstock and its impact on biodiesel emission characteristics. *Environ. Prog. Sustain. Energy*, 37, 7-19.
Kong, X., Zhu, Y., Zheng, H., Zhu, Y., Fang, Z., 2017. Inclusion of Zn into Metallic Ni Enables Selective and Effective Synthesis of 2,5-Dimethylfuran from Bioderived 5-Hydroxymethylfurfural. *ACS Sustain. Chem. Eng.*, 5, 11280-11289.
Kumar, A., Zo, S.M., Kim, J.H., Kim, S.C., Han, S.S., 2019. Enhanced physical, mechanical, and cytocompatibility behavior of polyelectrolyte complex hydrogels by reinforcing halloysite nanotubes and graphene oxide. *Compos. Sci. Technol.*, 175, 35-45.
Li, J., Zhou, M., Ye, Z., Wang, H., Ma, C., Huo, P., Yan, Y., 2015a. Enhanced photocatalytic activity of g-C_3N_4-ZnO/HNT composite heterostructure photocatalysts for degradation of tetracycline under visible light irradiation. *RSC Adv.*, 5, 91177-91189.
Li, X., Yao, C., Lu, X., Hu, Z., Yin, Y., Ni, C., 2015b. Halloysite–CeO2–AgBr nanocomposite for solar light photodegradation of methyl orange. *Appl. Clay Sci.*, 104, 74-80.
Ma, H., Ma, W., Chen, J.-F., Liu, X.-Y., Peng, Y.-Y., Yang, Z.-Y., Tian, H., Long, Y.-T., 2018. Quantifying Visible-Light-Induced Electron Transfer Properties of Single Dye-Sensitized ZnO Entity for Water Splitting. *J. Am. Chem. Soc.*, 140, 5272-5279.
Massaro, M., Buscemi, G., Arista, L., Biddeci, G., Cavallaro, G., D'Anna, F., Di Blasi, F., Ferrante, A., Lazzara, G., Rizzo, C., Spinelli, G., Ullrich, T., Riela, S., 2019a. Multifunctional Carrier Based on Halloysite/Laponite Hybrid Hydrogel for Kartogenin Delivery. *ACS Med. Chem. Lett.*, 10, 419-424.
Massaro, M., Campofelice, A., Colletti, C.G., Lazzara, G., Noto, R., Riela, S., 2018a. Functionalized halloysite nanotubes: Efficient carrier systems for antifungine drugs. *Appl. Clay Sci.*, 160, 186-192.
Massaro, M., Colletti, C.G., Buscemi, G., Cataldo, S., Guernelli, S., Lazzara, G., Liotta, L.F., Parisi, F., Pettignano, A., Riela, S., 2018b. Palladium nanoparticles immobilized on halloysite

nanotubes covered by a multilayer network for catalytic applications. *New J. Chem.*, 42, 13938-13947.
Massaro, M., Colletti, C.G., Fiore, B., La Parola, V., Lazzara, G., Guernelli, S., Zaccheroni, N., Riela, S., 2019b. Gold nanoparticles stabilized by modified halloysite nanotubes for catalytic applications. *Appl. Organomet. Chem.*, 33.
Massaro, M., Colletti, C.G., Guernelli, S., Lazzara, G., Liu, M., Nicotra, G., Noto, R., Parisi, F., Pibiri, I., Spinella, C., Riela, S., 2018c. Photoluminescent hybrid nanomaterials from modified halloysite nanotubes. *J. Mater. Chem. C*, 6, 7377-7384.
Massaro, M., Colletti, C.G., Lazzara, G., Milioto, S., Noto, R., Riela, S., 2017. Halloysite nanotubes as support for metal-based catalysts. *J. Mater. Chem. A*, 5, 13276-13293.
Massaro, M., Riela, S., 2018. Organo-clay nanomaterials based on halloysite and cyclodextrin as carriers for polyphenolic compounds. *J. Funct. Biomater.*, 9.
Massaro, M., Riela, S., Cavallaro, G., Colletti, C.G., Milioto, S., Noto, R., Lazzara, G., 2016. Ecocompatible Halloysite/Cucurbit[8]uril Hybrid as Efficient Nanosponge for Pollutants Removal. *ChemistrySelect*, 1, 1773-1779.
Mishra, G., Mukhopadhyay, M., 2019. TiO_2 decorated functionalized halloysite nanotubes (TiO_2 @HNTs) and photocatalytic PVC membranes synthesis, characterization and its application in water treatment. *Sci. Rep.*, 9.
Niu, F., Chen, D., Qin, L., Zhang, N., Wang, J., Chen, Z., Huang, Y., 2015. Facile Synthesis of Highly Efficient p–n Heterojunction CuO/BiFeO3 Composite Photocatalysts with Enhanced Visible-Light Photocatalytic Activity. *ChemCatChem*, 7, 3279-3289.
Shankar, S., Kasapis, S., Rhim, J.W., 2018. Alginate-based nanocomposite films reinforced with halloysite nanotubes functionalized by alkali treatment and zinc oxide nanoparticles. *Int. J. Biol. Macromol.*, 118, 1824-1832.
Sharma, S., Singh, A.A., Majumdar, A., Butola, B.S., 2019. Tailoring the mechanical and thermal properties of polylactic acid-based bionanocomposite films using halloysite nanotubes and polyethylene glycol by solvent casting process. *J. Mater. Sci.*, 54, 8971-8983.
Sidorenko, A.Y., Kravtsova, A.V., Aho, A., Heinmaa, I., Volcho, K.P., Salakhutdinov, N.F., Agabekov, V.E., Yu. Murzin, D., 2018. Acid-modified Halloysite Nanotubes as a Stereoselective Catalyst for Synthesis of 2H-Chromene Derivatives by the Reaction of Isopulegol with Aldehydes. *ChemCatChem*, 10, 3950-3954.
Ta, Q.T.H., Cho, E., Sreedhar, A., Noh, J.-S., 2019. Mixed-dimensional, three-level hierarchical nanostructures of silver and zinc oxide for fast photocatalytic degradation of multiple dyes. *J. Catal.*, 371, 1-9.
Tarasova, E., Naumenko, E., Rozhina, E., Akhatova, F., Fakhrullin, R., 2019. Cytocompatibility and uptake of polycations-modified halloysite clay nanotubes. *Appl. Clay Sci.*, 169, 21-30.
Wang, R., Jiang, G., Ding, Y., Wang, Y., Sun, X., Wang, X., Chen, W., 2011. Photocatalytic Activity of Heterostructures Based on TiO2 and Halloysite Nanotubes. *ACS Appl. Mater. Interf.*, 3, 4154-4158.
Yan, S., Salley, S.O., Simon Ng, K.Y., 2009. Simultaneous transesterification and esterification of unrefined or waste oils over ZnO-La_2O_3 catalysts. *Appl. Catal. A*, 353, 203-212.